Rhombohedral and Turbostratic Boron Nitride: X-ray Diffraction and Photoluminescence Signatures

Matthieu Moret, Adrien Rousseau, Pierre Valvin, Shashim Sharma, Laurent Souqui, Henrik B Pedersen, Hans Hogberg, Guillaume Cassabois, Jiahan Li, J. Edgar, et al.

Applied Physics Letters

Rhombohedral and turbostratic boron nitride: X-ray diffraction and photoluminescence signatures

Cite as: Appl. Phys. Lett. **119**, 262102 (2021); https://doi.org/10.1063/5.0076424
Submitted: 25 October 2021 • Accepted: 09 December 2021 • Published Online: 27 December 2021

Matthieu Moret, Adrien Rousseau, Pierre Valvin, et al.

Applied Physics Letters ARTICLE scitation.org/journal/apl

Rhombohedral and turbostratic boron nitride: X-ray diffraction and photoluminescence signatures

Cite as: Appl. Phys. Lett. **119**, 262102 (2021); doi: 10.1063/5.0076424
Submitted: 25 October 2021 · Accepted: 9 December 2021 ·
Published Online: 27 December 2021

Matthieu Moret,[1] Adrien Rousseau,[1] Pierre Valvin,[1] Sachin Sharma,[2] Laurent Souqui,[3] Henrik Pedersen,[2] Hans Högberg,[2] Guillaume Cassabois,[1] Jianhan Li,[4] J. H. Edgar,[4] and Bernard Gil[1,a)]

AFFILIATIONS

[1]Laboratoire Charles Coulomb, UMR 5221 CNRS-Université de Montpellier, F-34095 Montpellier, France
[2]Department of Physics, Chemistry and Biology (IFM), Linköping University, SE-58183 Linköping, Sweden
[3]Department of Material Sciences and Engineering, University of Illinois at Urbana-Champaign, Urbana, Illinois 61801, USA
[4]Tim Taylor Department of Chemical Engineering, Kansas State University, Manhattan, Kansas 66506, USA

Note: This paper is part of the APL Special Collection on Wide- and Ultrawide-Bandgap Electronic Semiconductor Devices.
[a)]**Author to whom correspondence should be addressed:** Bernard.gil@umontpellier.fr

ABSTRACT

Boron nitride (BN) layers with sp^2 bonding have been grown by metal organic chemical vapor deposition on AlN underlayers, which are deposited on c-plane sapphire substrates. Two different boron precursors were employed—trimethylboron and triethylboron—while ammonia was used as the nitrogen precursor. The BN obtained epitaxial BN films contain ordered rhombohedral (rBN) and partially ordered turbostratic (tBN) stackings as evidenced by x-ray diffraction analysis. We discriminatively identify the PL signatures of the rBN and tBN from those typical of the hexagonal (hBN) and Bernal stackings (bBN). The optical signature of tBN appears at 5.45 eV, and it intercalates between the two recombination bands typical of rBN at 5.35 eV (strong intensity) and 5.55 eV(weaker intensity). The analogs of the high intensity band at 5.35 eV in rBN sit at 5.47 eV for hBN and at 5.54 eV for bBN.

There is booming interest in varying the stacking arrangement of two-dimensional materials, such as graphene and transition metal dichalcogenides.[1] Varying the positions of the layers from their usual position relative to their adjacent layers changes the material's properties.[2] Such changes are feasible because of the relative weak bonds between the layers. These weak bonds make it possible to shift the layers from their most stable equilibrium positions. The weak interlayer bonds are in contrast to the strong intralayer bonds within the layers. The simplest two-dimensional material is graphene, which is formed by one stable monolayer of carbon atoms, a thin slice of graphite, with hexagonal rings formed by six carbon atoms.[3] These layers are usually stacked in an *AB* pattern, also known as Bernal stacking, in which the hexagonal rings are shifted in adjacent layers, so the carbon atoms in adjacent layers are not located directly above each other. The nonequilibrium rhombohedral structure is formed when there is an ABC stacking sequence of three layers each in unique lateral positions.[4]

A second widely studied two-dimensional material is hexagonal boron nitride (hBN). It typically has an AA' stacking sequence: the hexagonal rings in each layer are aligned on top of each other.[5] The atoms in adjacent layers are directly on top of each other and alternate between boron and nitrogen from layer to layer. Deviations from this stacking sequence have been predicted and observed experimentally. Chubarov *et al.*[6] reported that the rhombohedral BN (rBN or ABC stacking) is formed at the interface when BN is deposited at high temperatures (1500 °C) on sapphire substrates. Mosuang and Lowther,[7] Yu *et al.*,[8] Sponza *et al.*,[9] Cazorla and Gould,[10] and Gilbert *et al.*[11] predicted the energy differences between hBN and the various other possible stacking sequences for boron nitride. There, thus, exist several BN stacking sequences all with in-plane sp^2 bonding, which are characterized by similar cohesive energies.[7–11] Therefore, it is difficult to avoid forming multi-polymorphic layers. This can result in turbostratic turbostratic BN (tBN), in which the distribution of trigonal B_3N_3

hexagon layers is not strictly parallel, but they are roughly stacked parallel to each other with a random rotation and translation about the layer normal axis.[12] This creates many spatially extended interfacial defects more or less in a vein similar to those initially identified by Bourrellier *et al.*[13] They demonstrated that these are efficient carrier localization centers that trap the photogenerated carriers, *partially or fully washing out the near band edge phonon-assisted radiative recombination, depending on their concentrations*. Consequently, the PL spectra of such BN thin films are generally dominated by the radiative recombination of the photogenerated carriers at defects.[14–16] The PL spectra for specific stackings, namely, the hexagonal hBN or AA',[17,18] and the Bernal bBN or AB forms[19] of BN have been experimentally shown to match advanced theoretical predictions.[9]

Here, we investigate the PL of the ABC rhombohedral stacking in BN layers grown by chemical vapor deposition (CVD) on *c*-plane [the (001) plane] sapphire. The samples also contain turbostratic BN phase (tBN). We determine that the PL signatures of the rhombohedral BN stacking and its analog in turbostratic BN are distinct from those typical of the hexagonal and Bernal stackings.

Al_2O_3 (001) epi-ready 330 μm-thick on-axis sapphire substrates, which were provided by the Roditi International Corp. Ltd., London, UK, were used. To support the growth of the boron nitride layer,[6,20] an AlN buffer layer was formed *in situ* by exposing the substrate to ammonia (NH_3) during 10 min prior to deposition. Two different boron precursors were employed, trimethylboron (TMB) (99.99% purity, Voltaix/Air Liquide Advance Materials, FL, USA) and triethylboron (TEB) (semiconductor grade quality, from SAFC Hitech, MA, USA) while NH_3 (99.999%, further purified to remove residual water using a getter filter) was used as the nitrogen precursor. In the hot-wall CVD system, 5000 sccm purified H_2 was maintained during the processes as the carrier gas. The deposition times for TMB and TEB were 60 and 240 min. The longer time for TEB helped to compensate for the difference in deposition rates. The TEB process was conducted at 1500 °C, 70 mbar with a 642:1 NH_3/TEB ratio (NH_3 flow is 450 sccm). The TMB process was performed at 1400 °C and 50 mbar with a 966:1 NH_3/TMB ratio (NH_3 flow is 870 sccm). The optimization of the CVD process for each respective precursor has previously been reported.[6,20,21]

X-ray diffraction (XRD) recorded at room temperature, in the Bragg–Brentano ($\theta/2\theta$) configuration using a Bruker D8 Discover diffractometer with a VÅNTEC linear detector. To increase the detectivity, a simple Göbel mirror was used resulting in a non-monochromatic primary beam: ($Cu(K_{\alpha 1}+K_{\alpha 2})$) with some traces of $Cu(K_\beta)$ and W(LA1). In the case of purely oriented (001) BN films and in the $\theta/2\theta$ condition, only diffraction peaks at ∼27°, ∼55°, and ∼78° angles are expected.

Using pole figure measurements of the diffraction in such samples, the rhombohedral phase was detected as discussed in Ref. 20. The azimuthal scans (ϕ-scans) were acquired using a Phillips X'Pert MPD, cross-slits ($2 \times 2\,mm^2$) with a nickel K_β filter as primary optics and a proportional detector (PW1711/96) equipped with a parallel plate collimator.

The PL was excited using the 194 nm radiation of the fourth harmonics of a Ti-Sa laser. The hyperspectral PL microscopy in the deep-UV range was performed at cryogenic temperature (Tsample ∼6 K).

Figures 1 and 2 summarize the x-ray diffraction results. The main peaks from BN were detected as well as peaks from the AlN

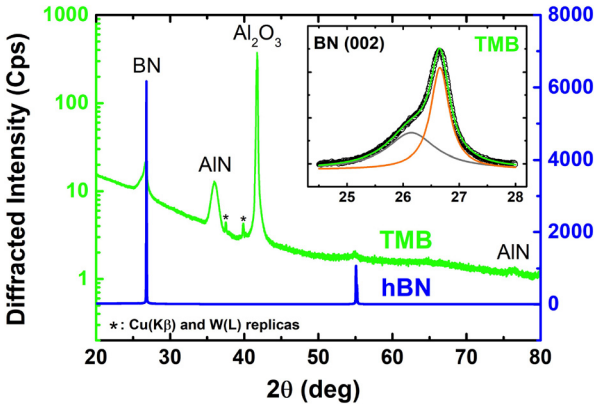

FIG. 1. $\theta/2\theta$ Diffractograms for sample TMB (green) and hBN (blue). Note the simultaneous recording of signal related to BN, to (001)-oriented AlN and sapphire. Inserted the line shape fitting of the BN-related diffraction showing the relative amounts of tBN (gray) and sp^2-BN orange) and their sum (green) compared to the experimental data (open black dots). The scales are represented in counts per second logarithmically in green at the left hand side for the epilayer, linearly in blue for the bulk test crystal, respectively.

buffer layer at 37° and the Al_2O_3 substrate at 42°. Interestingly, there are differences between the sharpness and intensities of the diffraction peaks from AlN. These differences are due to a size effect: the thinner the AlN film, the broader its extent in reciprocal space, according to Fourier analysis. The AlN buffer layer is, thus, thinner for the sample grown using TMB than for the sample grown using TEB. A more quantitative analysis can be made by carefully using the Scherrer formula[22,23] on the (002) AlN at $2\theta = 36.03°$ and with the assumption that the films are free of stresses. The coherent crystalline domains calculated from this formula are 9 nm [full width at half maximum (FWHM) = 0.90°] and 18 nm [FWHM = 0.45°] for the sample grown using TMB and TEB, respectively. The reason for thicker AlN growth

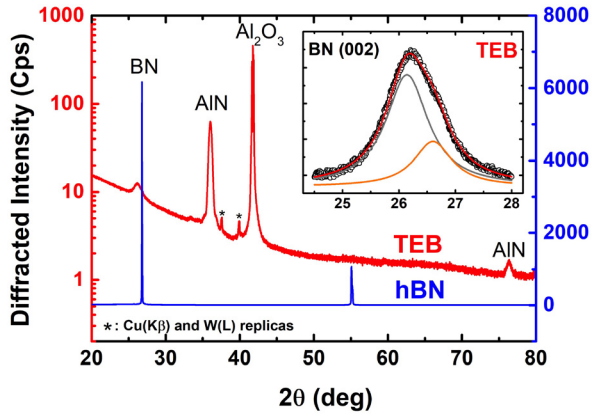

FIG. 2. $\theta/2\theta$ Diffractograms for sample TEB (red) and hBN (blue). Note the simultaneous recording of signal related to BN, to (001)-oriented AlN and sapphire. Inserted the line shape fitting of the BN-related diffraction showing the relative amounts of tBN (gray) and sp^2-BN (orange) and their sum (red) compared to the experimental data (open black dots). The scales are represented in counts per second logarithmically in red at the left hand side for the epilayer, linearly in blue for the bulk test crystal, respectively.

TABLE I. Summary of the line shape fitting of the composite diffraction peak in the 2θ angle range around 26°. The three left-hand columns of numerical data correspond to tBN while the four right-hand ones are for sp^2 BN.

	tBN (002)			sp^2 BN		
Precursor	Position (°)	FWHM (°)	Area (°.Cps)	Position (°)	FWHM (°)	Area (°.Cps)
TMB	26.15	1.05	6.62	26.66	0.40	7.07
TEB	26.14	0.91	4.43	26.61	0.82	1.61

on the film deposited from TEB is due to the nitridation and growth at higher temperature (1500 °C) compared to the film deposited from TMB at 1400 °C. The difference in growth conditions is a consequence of process optimization. TMB and TEB follow different chemical pathways to form BN films with NH_3 using metal organic chemical vapor deposition (MOCVD). Hence, the different precursors require different temperatures to form crystalline BN films. Thus, the higher growth temperature applied during growth the film with TEB explains the more favorable conditions for growth of crystalline AlN. In addition, this explains why the TEB sample has more tBN and which has a lower XRD intensity. The tendency for more tBN to form as the AlN buffer becomes thicker was previously described.[6,20,21]

Note the asymmetry of the diffraction peak near 26°, shown magnified in the insets of both Figs. 1 and 2. Two Gaussian functions, plotted in gray and orange, respectively, are required to fit the line shape centered around a diffraction angle typical of the periodic sp^2 BN stacking, namely, 26.6°–26.7° and around a diffraction angle of smaller value (typically 26.14°). Although the FWHM broadening of the lower diffraction angle (gray) feature is similar, of the order of 1° in both cases, the FWHM of the higher angle peak (shown in orange) varies. The higher the intensity of the lower (gray) peaks, the higher the value of the FWHM of the higher (orange) feature characteristic of the periodic boron nitride stacking. The full set of parameters obtained from the line shape fitting procedure is gathered in Table I. We interpret the x-ray diffraction feature at 26.14° as the signature of tBN stacking with an average value of the interlayer spacing of 0.341 nm [in tBN, the average stack height L_c of a parallel layer group consists of four to five layers while the average in-plane grain diameter (L_a) is considerably greater than the stack height[19]]. For the sake of completeness, we have inserted in blue in Figs. 1 and 2, the $\theta/2\theta$ diffraction feature of a typical thick hBN bulk crystal grown from a molten iron solution at atmospheric pressure,[24] hereafter labeled hBN. This standard sample was also used for the comparison of the PL features. Please note the number of counts per second (Cps), which for the thick bulk sample is on the order of 6000. The influence of the thickness of the AlN buffer layer seems to be more critical than the use of TMB or TEB.

The ϕ-scans displayed in Fig. 3 were used to confirm the epitaxial growth of the films deposited on the *c*-cut sapphire using the TMB precursor. As previously noted, there is twinning of the expected threefold symmetry of this rhombohedral system for the rBN planes; hence, six peaks from rBN are observed. The low intensity for a few peaks compared to others is due to the tilt sensitivity from tilting of the sample at particular ϕ angles.[6,20,21]

The XRD results motivate complementary PL experiments. As predicted by Sponza *et al.*[9] and verified by Rousseau *et al.*,[19] the AB Bernal stacking has a direct bandgap transition at 6.035 eV. Sponza *et al.*[9] predicted a lower bandgap value (by less than about 400 meV) for rBN. Based on the excellent theoretical predictions of this paper, we anticipate that the signature of rBN should appear at lower energies than those of AA' hBN and AB bBN stackings. In addition, we expect broad PL lines as we have no experimental evidence of a pure single phase in our samples.

In Fig. 4, the PL spectra of the TEB (red), TMB (green), and hBN (blue) samples are illustrated. The PL intensities from the TEB and TMB samples were similar while the PL of hBN was scaled so all three spectra can be compared. Weak residual emission peaks corresponding to AlN are recorded above 6 eV in the case of the epitaxial layers. For the bulk hBN crystal, instead of the traditional series of phonon-assisted transitions, there is just an onset of emission that rises near 5.9 eV corresponding to the E_{ix}-TA_T energy, which merges with defect-related emission that onsets near 5.7 eV. The PL bands in the epitaxial layers exhibit maxima at 5.35 and 5.55 eV, *with the lower energy feature dominating* and a couple of energies clearly different from what is observed in high quality bulk hBN crystals (5.62, 5.47, 5.32, and 5.17 eV). These two bands at 5.35 and 5.55 eV were previously reported for MBE-grown hBN on pyrolytic graphite samples.[25] In combination with their simultaneous appearance in the rBN x-ray diffraction pattern, they can be attributed to a rBN-related PL. We also recall that x-ray diffraction experiments performed on sample "C+Ni+Cr" of Ref. 19 revealed weak inclusions of rBN and no tBN.

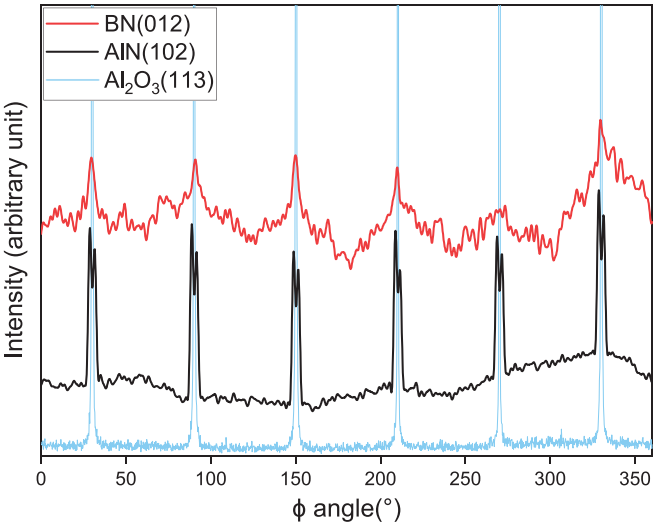

FIG. 3. XRD ϕ-scans from a film grown using TMB on c-cut sapphire confirming epitaxial growth between each layer seen from top to bottom r-BN{012} in red, AlN{102} in black, and Al_2O_3{113} in blue.

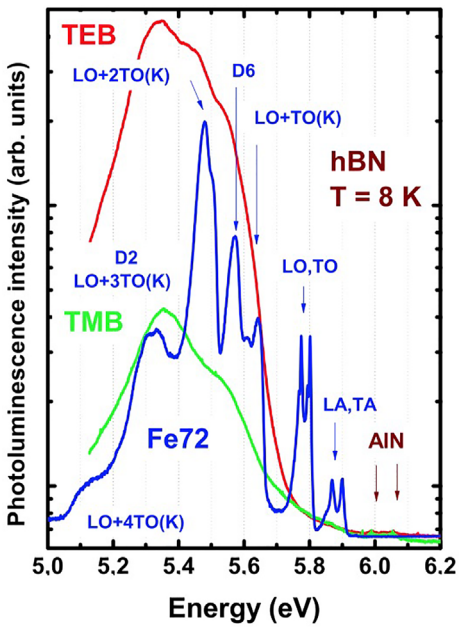

FIG. 4. Logarithmic plots of the PL recorded at 8 K for the TEB (red), TMB (green), and bulk hBN (blue plot) samples. Obviously the PL peak maximum is red-shifted compared to the bulk hBN case for the epilayers.

Therefore, the features at 5.55 and 5.35 eV in the PL spectrum of "C+Ni+Cr" (in orange), combined with those of hBN (blue) and the BN films prepared using TMB and TEB (green and red) in Fig. 5, profitably consolidate our interpretation of rBN properties. The PL emission from rBN is quite different from bulk hBN samples: In the latter cases, the defects responsible for the localized fluorescence are

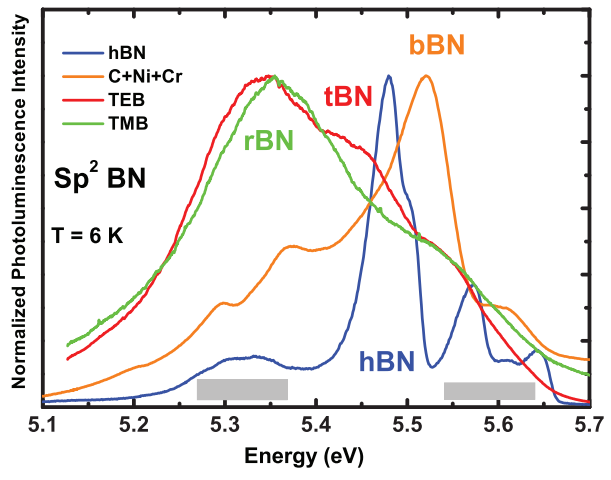

FIG. 5. Comparison between the low temperature PL spectra recorded in the 5.0 eV–6.0 eV range: (i) typical of a bulk hBN crystal[24] (blue), (ii) for a composite hBN, bBN, and rBN crystal[18] with bBN in dominating proportions (orange, sample "C+Ni+Cr" of the reference), and (iii) sp^2 BN layers described above in the paper (green and red). The gray rectangles indicate energy regions where is identified an overlap of the extrinsic defect-related PL with other contributions of unidentified origin in hBN.[28]

associated with specific folding of the surface layers of the hBN crystal.[13,26] The orientations of these folds are controlled by the crystallographic property of the hBN beneath them. PL and cathodoluminescence (CL) measurements reveal that emissions are due to a valley-orbit phonon interaction scattering involving the TO(K) phonon,[27] and a clear relationship is observed between the orientations of the light-emitting defects and the macroscopic crystal shape, and a 60° in-plane rotation with the number of TO(K) overtones.[17,26] The gray rectangles in Fig. 5 indicate the energy regions associated with an overlap of the extrinsic defect-related PL with other contributions of unidentified origin in hBN.[27,28]

In the case of the BN epitaxial films, we study here, as indicated in Fig. 6, a hyperspectral mapping of the PL intensity at the micrometer scale,[28] concretely indicating that the light is emitted with an intensity grossly homogeneous over the sample, regardless of the energy window chosen for imaging. Maps 6(a) to 6(c) are shown here in the case of sample TEB corresponding to integrations over three different energy regions, in spectral windows ranging between (5.3–5.35) eV, (5.4–5.45) eV, and (5.5–5.55) eV, respectively (indicated in Fig. 5). The maps size is $5 \times 5\ \mu m^2$ with 500 nm steps. The color map is the same for all the maps with a minimum (black) at 0 count·s^{-1} and a maximum (yellow) at 300 count·s^{-1}. The relationship between the colors and the PL intensity is indicated below the maps. A global PL spectrum integrated over the whole scanned area plot between 5.1 and 5.7 eV is offered in 6(d). The three shaded areas on the plot represent the energy regions where the PL maps (a) to (c) have been integrated. The bands/lines at 5.35 and 5.55 eV previously reported in the case of BN grown on sapphire by MBE[25] and MOCVD[29] are specific to the epitaxial layers. Probably, it is a result of the coalescence of the different nucleation centers. The defect concentrations that they are associated with are very high, which produces an efficient localization of all kinds of photo-created carriers and leads to the washing out of the high energy intrinsic emissions.

The presence of turbostraticity of the epitaxial films introduces some disorder-related broadenings of the PL lines like it does for the x-ray diffraction features, but an additional structure is observed at 5.45 eV for the TEB epilayer, which was dominated by tBN, as indicated by x-ray diffraction as seen in Fig. 2. We anticipate that from this, the shape of the PL from "pure" tBN should peak in the 5.45 eV region, as predicted theoretically by Mengle and Kioupakis.[30] Although here we are dealing with multiphasic structures (except hBN) and the PL bands are broad and overlapping, the conjunction of the optical responses, which is linked to the existence of many defects at interfaces of the different growth domains, with x-ray investigation, leads us to be quite confident with this interpretation. Said differently, the PL signature of tBN can only give a spectrally distributed band.

In conclusion, in relationship with their different x-ray diffraction features, we interpret the PL spectra of very high, state-of-the-art quality bulk hBN, with those of mixed hBN, rBN, and tBN of epitaxial films grown by CVD on AlN buffer layers of different thicknesses, deposited on a c-plane oriented sapphire substrate. Except for the ultra-pure sample, the PL spectra display a series of intricate broad bands that we could *only* interpret in terms of extrinsic recombination. The PL signature of tBN, which was never identified previously, appears at 5.45 eV, and it intercalates between the two recombination bands typical of rBN at 5.35 eV (strong intensity) and 5.55 eV (weaker intensity) that were already reported for BN epilayers grown by MBE

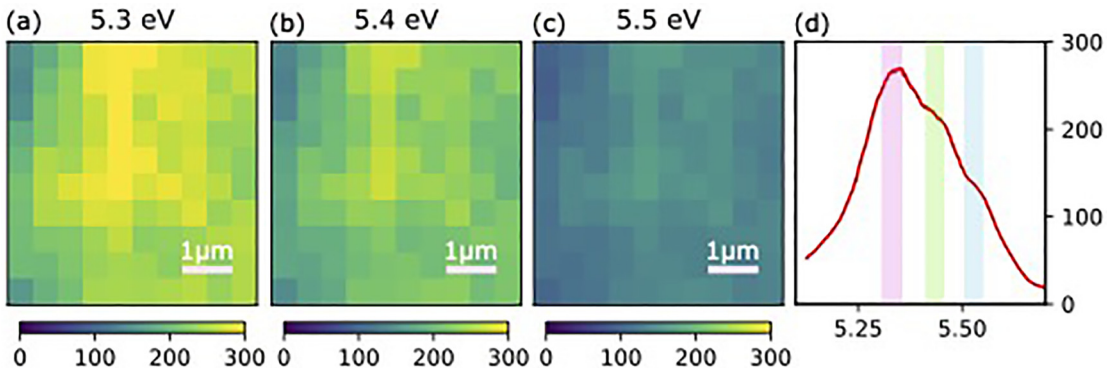

FIG. 6. The hyperspectral PL microscopy at 6 K for sample TEB. Maps (a) to (c) correspond to integrations over different three energy regions, in spectral windows ranging between (5.3–5.35) eV, (5.4–5.45) eV, and (5.5–5.55) eV, respectively. The size of the maps is 5 × 5 μm^2 with 500 nm steps. The color map is the same for all the maps with a minimum (black) at 0 count·s^{-1} and a maximum (yellow) at 300 count·s^{-1}. The relationship between the colors and the PL intensity in the maps indicated below. A global PL spectrum integrated over the whole scanned area plot between 5.1 and 5.7 eV is offered in (d). The three shaded areas on the plot represent the energy regions where the PL maps (a) to (c) have been integrated.

and CVD. These results are in concert with what is routinely reported in hBN and integrates within time passing among the successive examinations by Silly *et al.*,[14] Jaffrenou *et al.*,[15] Museur *et al.*,[16] and by Bourrelier *et al.*[13,26] and complete them toward the progressive and final understanding of the PL of BN below 5.73 eV in terms of the localized various sp^2 BN stackings departing from the AA′ hexagonal one. Through all the series of stackings examined here, Bernal boron nitride exhibits an extrinsic PL peak at a maximum highest energy of 5.54 eV, which is also seen in the epilayers. This statement remains in the domain of the bona fide feeling at the time being, since, unfortunately, x-ray diffraction information does not reveal pure bBN and rBN monophasic bulk crystals of high enough dimensions to offer less broadened features including when using our micro-PL probe with its the spatial resolution (200 nm). The PL signature of tBN at 5.45 eV is also of extrinsic origin.

The authors gratefully acknowledge C. L'Henoret and T. Cohen for their technical support at the mechanics workshop. This paper was financially supported by the network GaNeX (ANR-11-LABX-424 0014), the BONASPES project (ANR-19-CE30 0007), the ZEOLIGHT project (ANR-19-CE08-0016), and the Université de Montpellier. S.S. and L.S. acknowledge financial support from the Swedish Research Council Contract No. 2017-04164, and the Swedish Foundation for Strategic Research (SSF), Contract No. IS14-0027, and Carl Trygger's Foundation for Scientific Research, Contract No. CTS 14:189, respectively. H.P. and H.H. acknowledge the Swedish Government Strategic Research Area in Materials Science on Advanced Functional Materials at Linköping University (Faculty Grant SFO-Mat-LiU No. 2009-00971). Support for BN crystal growth came from the Office of Naval Research under Award No. N00014-20-1-2474, 428 and the National Science Foundation under Award No. CMMI 429 #1538127.

AUTHOR DECLARATIONS

Conflict of Interest

The authors have no conflicts to disclose.

DATA AVAILABILITY

The data that support the findings of this study are available from the corresponding author upon reasonable request.

REFERENCES

[1]A. K. Geim and I. V. Grigorieva, Nature **499**, 419 (2013).
[2]F. Withers, O. Del Pozo-Zamudio, A. Mishchenko, A. P. Rooney, A. Gholinia, K. Watanabe, T. Taniguchi, S. J. Haigh, A. K. Geim, A. I. Tartakovskii, and K. S. Novoselov, Nat. Mater. **14**, 3101 (2015).
[3]K. S. Novoselov, A. K. Geim, S. V. Morozov, D. Jiang, Y. Zhang, S. V. Dubonos, I. V. Grigorieva, and A. A. Firsov, Science **306**, 666–669 (2004).
[4]R. Setton, "Carbon, a fundamental element for research and its applications," in *Carbon Molecules and Materials*, edited by R. Setton, P. Bernier, and S. Lefran (Taylor & Francis, London/New York, 2002).
[5]R. S. Pease, Acta Cryst. **5**, 356 (1952).
[6]M. Chubarov, H. Pedersen, H. Högberg, J. Jensen, and A. Henry, Cryst. Growth Des. **12**, 3215 (2012).
[7]T. E. Mosuang and J. E. Lowther, J. Phys. Chem. Solids **63**, 363 (2002).
[8]W. J. Yu, W. M. Lau, S. P. Chan, Z. F. Liu, and Q. Q. Zheng, Phys. Rev. B **67**, 014108 (2003).
[9]L. Sponza, H. Amara, C. Attaccalite, S. Latil, T. Galvani, F. Paleari, L. Wirtz, and F. Ducastelle, Phys. Rev. B **98**, 125206 (2018).
[10]C. Cazorla and T. Gould, Sci. Adv. **5**, eaau5832 (2019).
[11]S. M. Gilbert, T. Pham, M. Dogan, S. Oh, B. Shevitski, G. Schumm, S. Liu, P. Ercius, S. Aloni, M. L. Cohen, and A. Zettl, 2D Mater. **6**, 021006 (2019).
[12]J. Thomas, Jr., N. E. Weston, and T. E. O'Connor, J. Am. Chem. Soc. **84**, 4619 (1962).
[13]R. Bourrellier, M. Amato, L. H. G. Tizei, C. Giorgetti, A. Gloter, M. I. Heggie, K. March, O. Stéphan, L. Reining, M. Kociak, and A. Zobelli, ACS Photonics **1**, 857 (2014).
[14]M. G. Silly, P. Jaffrennou, J. Barjon, J.-S. Lauret, F. Ducastelle, A. Loiseau, E. Obraztsova, B. Attal-Tretout, and E. Rosencher, Phys. Rev. B **75**, 085205 (2007).
[15]P. Jaffrennou, J. Barjon, J.-S. Lauret, B. Attal-Trétout, F. Ducastelle, and A. Loiseau, J. Appl. Phys. **102**, 116102 (2007).
[16]L. Museur, E. Feldbach, and A. Kanaev, Phys. Rev. B **78**, 155204 (2008).
[17]G. Cassabois, P. Valvin, and B. Gil, Nat. Photonics **10**, 262 (2016).
[18]T. Q. P. Vuong, G. Cassabois, P. Valvin, V. Jacques, A. V. Der Lee, A. Zobelli, K. Watanabe, T. Taniguchi, and B. Gil, 2D Mater. **4**, 011004 (2016).
[19]A. Rousseau, M. Moret, P. Valvin, W. Desrat, J. H. Edgar, G. Cassabois, and B. Gil, Phys. Rev. Mater. **5**, 064602 (2021).
[20]M. Chubarov, H. Pedersen, H. Högberg, A. Henry, and Z. Czigány, J. Vac. Sci. Technol. A Vac. Surf. Films **33**, 061520 (2015).
[21]L. Souqui, H. Pedersen, and H. Högberg, J. Vac. Sci. Technol. A **37**, 020603 (2019).
[22]A. Patterson, Phys. Rev. **56**, 978 (1939).
[23]A. K. Dabrowska, M. Tokarczyk, G. Kowalski, J. Binder, R. Bozek, J. Borysiuk, R. Stepniewski, and A. Wysmołek, 2D Mater. **8**, 015017 (2020).
[24]J. Li, J. Wang, X. Zhang, C. Elias, G. Ye, D. Evans, G. Eda, J. M. Redwing, G. Cassabois, B. Gil, P. Valvin, R. He, B. Liu, and J. H. Edgar, ACS Nano **15**, 7032 (2021).

[25]T. Q. P. Vuong, G. Cassabois, P. Valvin, E. Rousseau, A. Summerfield, C. J. Mellor, Y. Cho, T. S. Cheng, J. D. Albar, L. Eaves, C. T. Foxon, P. H. Beton, S. V. Novikov, and B. Gil, 2D Mater. **4**, 021023 (2017).
[26]R. Bourrellier, Ph.D. thesis (University of Paris- Sud XI, 2014).
[27]G. Cassabois, P. Valvin, and B. Gil, Phys. Rev. B **93**, 035207 (2016).
[28]P. Valvin, T. Pelini, G. Cassabois, A. Zobelli, J. Li, J. H. Edgar, and B. Gil, AIP Adv. **10**, 075025 (2020).
[29]X. Z. Du, J. Li, J. Y. Lin, and H. X. Jiang, Appl. Phys. Lett. **108**, 052106 (2016).
[30]K. A. Mengle and E. Kiuoupakis, APL Mater. **7**, 021106 (2019).